

EFFECTS OF PULSATING FLOW CONDITIONS ON MIXED FLOW TURBINE PERFORMANCE

Li Chen, Weilin Zhuge, Yangjun Zhang, Lei Xie
State Key Laboratory of Automotive Safety and Energy
Tsinghua University
Beijing 100084, China
cl-05@mails.tsinghua.edu.cn

Shuyong Zhang
National Key Laboratory of
Diesel Engine Turbocharging Technology
Datong, Shanxi 037036, China

Abstract

Turbines work under actual pulsating flow conditions due to the operating characteristics of a reciprocating internal combustion engine. The pulsating flow conditions affect the flow fields in a turbine, and lead to obvious difference between actual and steady performance. A three-dimensional numerical investigation into mixed flow turbine under different kinds of pulsating flow conditions was conducted, in order to get an inner sight of the unsteady impact. The effects of the pulsation frequency and amplitude on the turbine performance were analyzed. The results show that the period average performance of the turbine under pulsating conditions is lower than the steady performance under the mean pulsating conditions. The actual power output varies little with the pulsation frequency changing, while the phase lag increases as the pulsation frequency increases. The unsteady characteristics become more obvious when the pulsation amplitude increases. Under the pulsating flow conditions, of which amplitude is 0.8, the period average efficiency is 4.11 percent lower than the steady efficiency. The flow fields fluctuate seriously under this high pulsating flow conditions. The occurrence and vanishing of the vortex are dynamic procedures, and hysteresis effect is observed in the unsteady flow.

1 INTRODUCTION

Oil remains the world largest energy source, and it accounts for 33.2% [1] of the world total primary energy supply in 2008. Transport is the world's fastest growing form of energy use [2]. It shows that transport accounts for about 61.4% of world oil consumption in 2008, which has increased significantly from 45.3% in 1973 [1]. On the other hand, greenhouse gases like carbon dioxide (CO₂) have been increasing over the past decades, and this leads to more apparent impact on the world environment and climate. Economic growth contributes to the increasing demand for

transport. In 2008 the transport produced nearly 22% of the global CO₂ emissions [3]. Global demand for transport appears unlikely to decrease in the foreseeable future; it is projected that transport will grow by 45% by 2030 [4].

The internal combustion engine (ICE) is the most common powertrain technology for load transportation. Therefore improving the efficiency of ICE is an effective way to reduce world fuel consumption and CO₂ emissions. Actually only about 25 percent of the energy contained in the fuel is converted into net power and delivered to the wheels, while other about one third of the energy is lost within exhaust [5]. These proportions may vary with different vehicle or engine types and operating conditions, but they give a good view of where gains can be achieved to improve the overall engine thermal efficiency and reduce CO₂ emission.

The energy in the exhaust is considerable, so it is reasonable to recover energy from the exhaust and improve the engine efficiency. The ICE waste heat recovery technologies, like turbocharging and turbocompounding, are widely studied and applied nowadays. In these applications, turbines are commonly used to extract energy from the exhaust then drive compressor or generator. The performance of the turbine will directly determine the efficiency of the waste heat recovery system, further influence the performance of ICE. Therefore, good aerodynamic performance of turbine is apparently demanded for an efficient ICE with waste heat recovery system.

Actually, turbines are under natural pulsating flow conditions due to the operating characteristics of a reciprocating internal combustion engine. This leads to a more complex and unsteady flow in a turbine. Until now, there have been some effective experimental and numerical studies of the performance of turbines under pulsating conditions [6-10], and showed occurrence of significant deviation of steady and actual

performance of the turbine, while the instantaneous efficiency formed a loop around the steady efficiency. Therefore, the approach of evaluating the behaviors within a turbine under steady or quasi-steady flow conditions may be handy and simple.

The volute prior to the rotor has significant influence to the unsteady behavior under pulsating flow conditions. On one hand the volume of volute has “filling and emptying” effect; on the other hand the geometry of the volute and rotating of rotor cause complex flow around the periphery of the rotor. It is reasonable to model the full rotor stage and the volute, even together with the manifold, in numerical simulations. However in such cases, the total mesh number would easily reach dozens of million level, when a dependable mesh density is employed. The unsteady simulation with such a mesh will requires substantial computation resources, and the computing time is normally unacceptable.

Although the volute has effects on the flow entering the rotor, the rotor is still exposed to pulsating flow[11]. It is necessary to evaluate the dynamic behavior in the rotor under pulsating flow conditions. Here in this paper, the numerical simulation model of the mixed flow turbine rotor was built and performed under different kinds of pulsating conditions. The effects of the pulsation frequency, amplitude on the turbine performance and flow fields were analyzed.

2 NUMERICAL METHOD

The computational fluid dynamics code NUMECA has been applied. The Navier-Stokes equations for the relative velocities in a rotating frame can be expressed as:

$$\frac{\partial \vec{U}}{\partial t} + \nabla \vec{F}_I + \nabla \vec{F}_V = \vec{Q}$$

Where \vec{U} is the vector of the conservative variables, \vec{F}_I and \vec{F}_V are respectively the inviscid and viscous flux vectors:

$$U = \begin{bmatrix} \rho & \rho W_x & \rho W_y & \rho W_z & \rho E \end{bmatrix}$$

$$\vec{F}_I = F_{Ix} \vec{i} + F_{Iy} \vec{j} + F_{Iz} \vec{k}, \quad \vec{F}_V = F_{Vx} \vec{i} + F_{Vy} \vec{j} + F_{Vz} \vec{k}$$

$$F_{Ii} = \begin{bmatrix} \rho W_i \\ P \delta_{xi} + \rho W_i W_x \\ P \delta_{yi} + \rho W_i W_y \\ P \delta_{zi} + \rho W_i W_z \\ (\rho E + P) W_i \end{bmatrix}, \quad -F_{Vi} = \begin{bmatrix} 0 \\ \tau_{ix} \\ \tau_{iy} \\ \tau_{iz} \\ q_i + W_z \tau_{iz} + W_y \tau_{iy} + W_x \tau_{ix} \end{bmatrix}$$

$$\delta_{ij} = \begin{cases} 1, & i = j \\ 0, & i \neq j \end{cases}$$

The stress and the heat flux components are given by:

$$q_i = \kappa \frac{\partial T}{\partial X_i},$$

$$\tau_{ij} = \mu \left(\frac{\partial W_i}{\partial X_j} + \frac{\partial W_j}{\partial X_i} - \frac{2}{3} (\nabla \cdot \vec{W}) \delta_{ij} \right)$$

The source term vector \vec{Q} contains contributions of Coriolis and centrifugal forces and is given by

$$Q = \begin{bmatrix} 0 \\ -\rho [2\vec{\omega} \times \vec{W} + (\vec{\omega} \times (\vec{\omega} \times \vec{r}))] \\ \rho \vec{W} \cdot \vec{\nabla} \left(\frac{1}{2} \omega^2 r^2 \right) \end{bmatrix}$$

Sparlart-Allmaras[12] turbulence model has been applied in order to get good accuracy and computing efficiency. The flow solver is based on a cell centred finite volume approach, associated with Jameson's center scheme as space discretization together with an explicit Runge-Kutta time integration method.

The dual time stepping approach was applied for the unsteady calculations, which consists in adding to the time dependent Navier-Stokes equations pseudo-time derivative terms. At each physical time step, a steady state problem is solved in a pseudo time and all available acceleration techniques such as multigrid, local time stepping and implicit residual smoothing can be applied. Then for unsteady flow simulations the Reynolds-Average Navier-Stokes equations can be expressed as:

$$\frac{\partial}{\partial t} \iiint_V U dV + \iiint_V \frac{\partial U}{\partial \tau} dV + \iint_S \vec{F} \cdot d\vec{S} = \iiint_V ST dV$$

Where t is the physical time and τ is the pseudo time, ST are the source terms.

At the inlet boundary of the numerical model, the absolute total pressure, total temperature and direction of the absolute velocity were imposed. Given that the rotor was accommodated in a nozzleless volute, the direction of the absolute velocity vector was obtained from the one-dimensional flow analysis of the volute [13, 14]. The ideal one-dimensional model of volute flow is based incompressible flow theory with constant angular momentum. The inlet flow angle was derived by the following equation.

$$\alpha_1 = \arctan \frac{\pi (r_{1hub} + r_{1tip}) b_1 / \left(\frac{r_{1hub} + r_{1tip}}{2} \right)}{A_0 / r_0} \quad (1)$$

$$= \arctan \frac{2\pi b_1}{A_0 / r_0} = 75^\circ$$

Where A_0 and r_0 are the area and mean radius of the volute inlet; A_1 and r_1 are the inlet area and radius of the rotor respectively; b_1 is the height of blade leading edge.

Different kinds of inlet total pressure boundary were given in the simulations, in order to investigate the effect of the pulsating conditions on the turbine. The total pressure imposed has certain average value and varies in certain amplitude with

sinusoidal function. It should be noticed that the actual exhaust pulse of the ICE is not simply following sinusoidal function. Here giving the sinusoidal pulsation is in a simplified consideration, and this would be more easier to discuss the effects of different pulsation characteristics.

The simulative pulsations of total pressure at the inlet with different frequencies and amplitudes are shown in Fig.1(a) and (b) respectively. The abbreviations “Fre”, “Pr”, “Amp” in the legend represent pulsating frequency, average expansion ratio and pulsating amplitude respectively. The parameter “Amp” is defined as:

$$\text{Amp} = \frac{p_{01,\max} - p_{01,\min}}{2 \cdot (p_{01,\text{ave}} - p_2)} \quad (2)$$

Where $p_{01,\max}$, $p_{01,\min}$ and $p_{01,\text{ave}}$ are the maximum, minimum and average value of the instantaneous inlet total pressure, and p_2 is outlet static pressure.

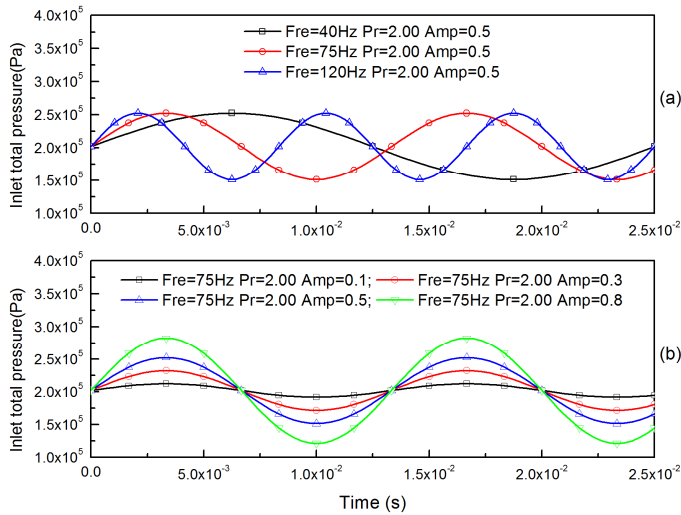


Fig.1 Absolute pressure imposed at the inlet

At the outlet boundary, the static pressure is assumed to be uniform in the tangential direction and the static pressure at a specific radius is given. The pressure distribution in the outlet section is then found by integrating the following equation:

$$\frac{\partial p}{\partial r} = \rho \cdot \frac{V_\theta^2}{r}$$

The remaining dependent variables on the outlet boundary are obtained from the interior field through extrapolation. Adiabatic and no-slip solid wall boundary conditions are imposed.

The numerical method introduced above was validated by the experiment data of Imperial College fourth generation mixed flow turbine (Turbine D)[15]. The time-average inlet total temperature and outlet static pressure were imposed, and the inlet total pressure was given varying with time. All these parameters were directly from the experiment data. The

comparisons of the predicted and experimental results under 20Hz pulsation at 80% equivalent speed are illustrated in Fig.2.

Reasonable agreement is observed between predicted and experimental performance, though there is obvious phase shift between the predicted and experimental torque traces.

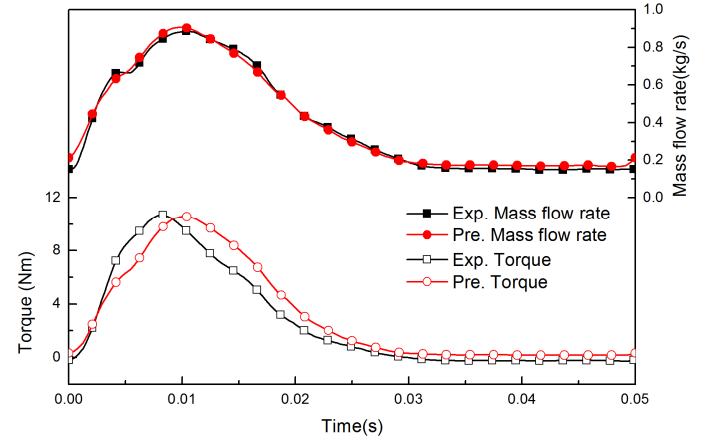


Fig.2 Comparisons of the predicted and experimental data

3 GEOMETRY AND GRIDS

The meridional and 3D view of the mixed flow turbine rotor simulated in this paper is shown in Fig.3, and the geometry details are listed in Tab.1. Only the rotor stage is simulated without the volute, and the computational grids are plotted in Fig.4. Periodic boundaries have been applied, thus only one blade passage has been modeled. The inlet and exit boundary conditions have been projected about two-thirds axial chord from the turbine leading and trailing edges. Structured hexahedron multi-block topology is employed, and the grids consist of a total of 9 mesh blocks leading to overall 789,980 grid points, which is a high mesh density for single passage simulation. H-topology is used in the inlet, outlet and main flow passage domains, whilst C-topology is used around the blade. The grid is refined at the near-wall, leading and trailing edge, and the y^+ value is controlled less than 5 in order to properly capture the high gradients inside the boundary layer.

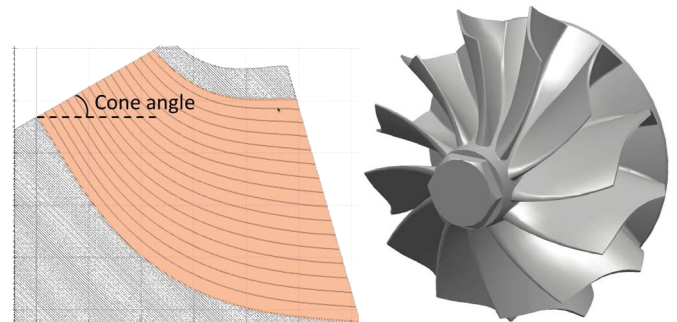


Fig.3 Geometry of the mixed flow turbine

Tab.1 Geometric details of the turbine

Parameter	Value
Inlet tip diameter	136.2 mm
Inlet hub diameter	114.7 mm
Outlet tip diameter	117.3 mm
Outlet hub diameter	35.3 mm
Tip gap height	0.6 mm
Cone angle	30°
Number of blades	12

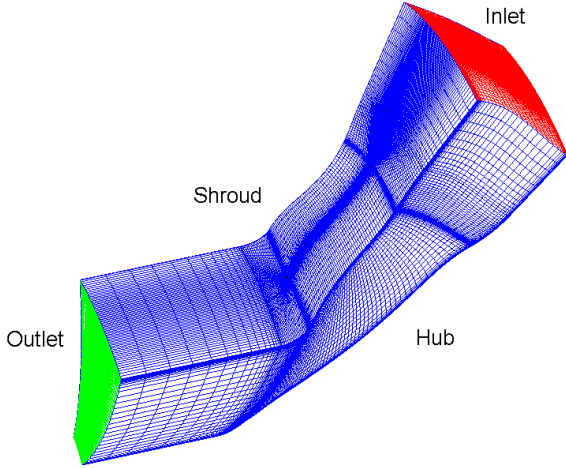


Fig.4 Computational grids of the turbine

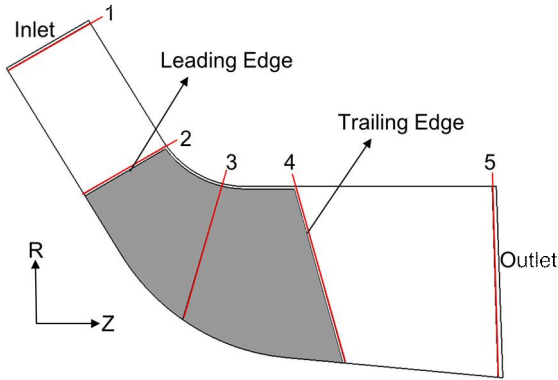


Fig.5 Passage cross sections

4 RESULTS AND DISCUSSION

The simulations of the turbine running at 50,000 rev/min under pulsating flow conditions, shown in Fig.1, were performed. The unsteady computations that restarted from fine convergent steady solutions, reached considerable periodic conditions after three full pulse periods, and ran finally about four full periods. The difference between mass flow rate at inlet and outlet is less than 3%, which is an acceptable error since take the time lag into account.

4.1 Propagation of disturbance

The pulsation imposed at the inlet boundary propagates through the turbine. This results in a finite time lag between the parameters traces measured at different locations in the turbine. This would be an issue when the instantaneous turbine efficiency is calculated, because the power output is calculated from the force on the blade while the isentropic power is calculated from the parameters at the inlet and outlet. In order to correct the time lag, the propagation speed of the parameters, like energy, should be evaluated. Several approaches have been employed by the researchers, that were sonic velocity approach[8, 11, 16], bulk flow approach[17, 18] and bulk flow plus sonic velocity approach[19-21].

For the purpose of evaluating the propagation of the disturbance, an unsteady computation with a short physical time step was conducted. The inlet pulse frequency, average expansion ratio and amplitude are 75Hz, 1.72 and 0.5 respectively, as shown in Fig.1. The physical time step is 6.667×10^{-5} s, that means 200 time steps are computed in a pulse period.

The variations of the weighted average value of different parameters at 5 cross sections are presented in Fig.6. The 5 passage cross sections chosen, which are near inlet, leading edge, middle of chord, trailing edge and outlet respectively, are shown in Fig.5. The weighted average value of the section is derived by equation(3).

$$\bar{q} = \frac{\int q \cdot \rho \cdot \vec{W} \cdot d\vec{S}}{\int \rho \cdot \vec{W} \cdot d\vec{S}} \quad (3)$$

The instantaneous isentropic work is calculated from the weighted average instantaneous total temperature and total pressure on each section, together with period average outlet static pressure:

$$P_{ise,ins} = \dot{m}_{ins} c_p \bar{T}_{0i,ins} \left[1 - \left(\frac{\bar{P}_{out}}{\bar{P}_{0i,ins}} \right)^{\frac{\gamma-1}{\gamma}} \right] \quad (4)$$

When P_{ise} is isentropic work; \dot{m} is mass flow rate; c_p is specific heat capacity at constant pressure; T is temperature, p is pressure; the subscript *ins*, 0, *i* denote instantaneous value, stagnation condition, and number of the cross section respectively. c_p and γ are assumed constant in the computation.

It is shown clearly in Fig.6 that the parameters vary obviously across the blade passage, and there exists a time lag as the disturbance propagating. Since the pulsating boundary imposed at the inlet is following sinusoidal function, the parameters on the sections have similar trend. Therefore the difference of the time when first crest/trough appears would be assumed to be the parameter time lag. The physical time step numbers when the first crest/trough appear and time lag of the parameters between the inlet and outlet are given in Tab.2.

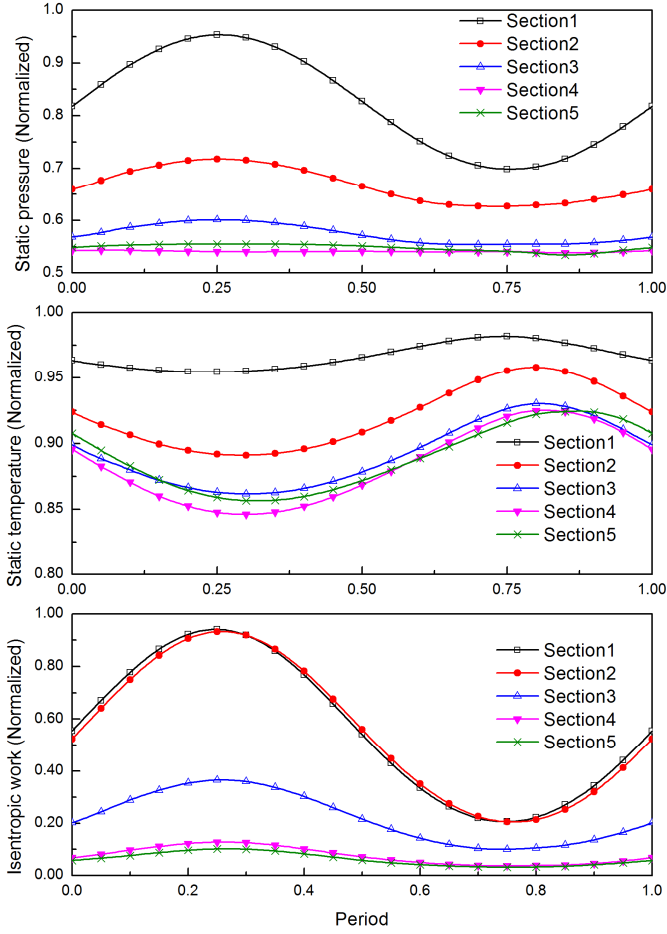


Fig.6 Disturbance on the cross sections in one period

Tab.2 Time lag of the parameters

Parameter	Pressure	Temperature	Isentropic work
Inlet(step)	51/200	48/200	50/200
Outlet(step)	56/200	64/200	53/200
Lag(step)	5/200	16/200	3/200
Time lag(s)	3.33×10^{-4}	1.07×10^{-3}	2.00×10^{-4}

Tab.3 Characteristic speed and time

	\bar{W}_m	\bar{c}	$\bar{c} + \bar{W}_m$
Speed(m/s)	138.69	549.72	688.41
Time(s)	9.58×10^{-4}	2.42×10^{-4}	1.93×10^{-4}

In order to evaluate the propagation speed of the disturbance, three characteristic speeds were calculated, that are average meridional velocity (\bar{W}_m), local sonic speed (\bar{c}), and $\bar{W}_m + \bar{c}$. All the values were averaged from the 5 cross sections:

$$\bar{c} = \frac{\sum_1^5 \bar{c}_i}{5}, \quad \bar{W}_m = \frac{\sum_1^5 \bar{W}_{m,i}}{5} \quad (5)$$

The meridional distance from the inlet to outlet at 50% span is about 132.83mm. The characteristic time, which derived from this distance and the characteristic speeds, is shown in Tab.3. Comparing the time lag in Tab.2 and the characteristic time in Tab.3, it is suggesting that the temperature disturbance propagates near bulk flow speed, and the pressure disturbance propagates near sonic speed, while the isentropic energy shows an even higher speed. Different parameters have different propagating procedures in the rotor, thus using a certain time to shift the parameters will not precisely correct the time lag. On the other hand, the power output is from the gases in the rotor, whilst the parameters measured at defined locations, like inlet or outlet, are time depended. Even if the time lag between different measure locations is corrected precisely, it still cannot represent all the gas in the rotor passage. Because that the gases in the passage driving the rotor are accumulated in finite time, but not in an instant. Consequently the turbine parameters are plotted as function of time in this paper, and time-averaged values are used to evaluate the mean performance.

4.2 Effects of pulsation on turbine performance

In order to investigate the effect of the pulsation frequency on the turbine performance, the simulations were performed under three pulsation frequencies while the pulsation amplitude (Amp=0.5) and average total pressure (Pr=2.0) were kept constant. The three pulsation frequencies were 40Hz, 75Hz and 120Hz, that are corresponding to a four-stroke, six cylinder engine running at 800, 1500 and 2400 rev/min respectively (for a single entrance volute turbine). The inlet total pressure imposed at the boundary is shown in Fig.1(a).

In order to capture enough flow phenomena in one pulsation period and take the computing efficiency into account, the physical time step was specified as one fortieth of the pulsation period long in these and the following computation cases. That means the physical step is depended on the pulsation frequency of the boundary, and 40 time steps are computed in each pulse period.

The actual power was calculated from the torque and angular velocity. Turbine torque was derived by integrating the element torque on the blade surface, as equation(6). The isentropic power was derived from the parameters at the inlet and outlet. In order to comparing the actual performance to steady performance under the mean conditions, a relative power value was calculated, which is the product of the instantaneous isentropic power and the steady efficiency under mean pulsating flow conditions.

$$M = \int_s \vec{r} \times (\vec{F} \cdot \vec{n}) ds \quad (6)$$

$$\bar{\eta} = \frac{\int_0^T P_{act} dt}{\int_0^T P_{ise} dt} = \frac{\int_0^T M \omega}{\int_0^T \dot{m} c_p T_{01} \left[1 - \left(\frac{P_2}{P_{01}} \right)^{\frac{\gamma-1}{\gamma}} \right]} \quad (7)$$

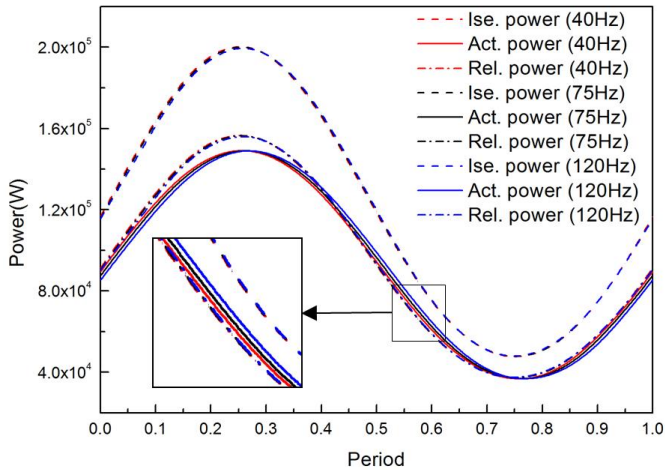


Fig.7 Instantaneous power under different pulsation frequencies

Plot the instantaneous power, isentropic power and relative power under different frequency pulsating flow conditions in Fig.7. The isentropic power values at a certain time are similar under the three frequencies, so that the three isentropic power traces almost overlap with each other. Since the relative power was calculated from isentropic power, they have the same phase. It is obvious that there is phase lag between the actual power and isentropic power. The phase lag increases as the pulsation frequency increases. Taking the phase lag into consideration, the actual power output varies little with the pulsation frequency changing. Near the 1/4 period time, the difference between actual power and relative power is largest. This caused by two reasons, firstly the isentropic work is larger in this time region, secondly the instantaneous performance of the turbine is much worse than the steady performance under the mean pulsation conditions.

The time-average efficiency under pulsating conditions was calculated by equation (7) to evaluate the cycle average performance, given in Tab.4. $\Delta\eta$ is the deviation of the unsteady time-average efficiency from the steady efficiency under pulse mean condition. The steady efficiency equals 78.17%. Tab.4 shows that the time-average efficiencies under different pulsation frequencies are similar, and they are all lower than the steady efficiency.

Tab.4 Time-average efficiency under different pulsation frequencies

Frequency	40Hz	75Hz	120Hz
$\bar{\eta}$	76.48%	76.50%	76.55%
$\Delta\eta$	-1.69%	-1.67%	-1.62%

Tab.5 Time-average efficiency under different pulsation amplitudes

Amplitude	0.1	0.3	0.5	0.8
$\bar{\eta}$	78.09%	77.52%	76.50%	74.06%
$\Delta\eta$	-0.08%	-0.65%	-1.67%	-4.11%

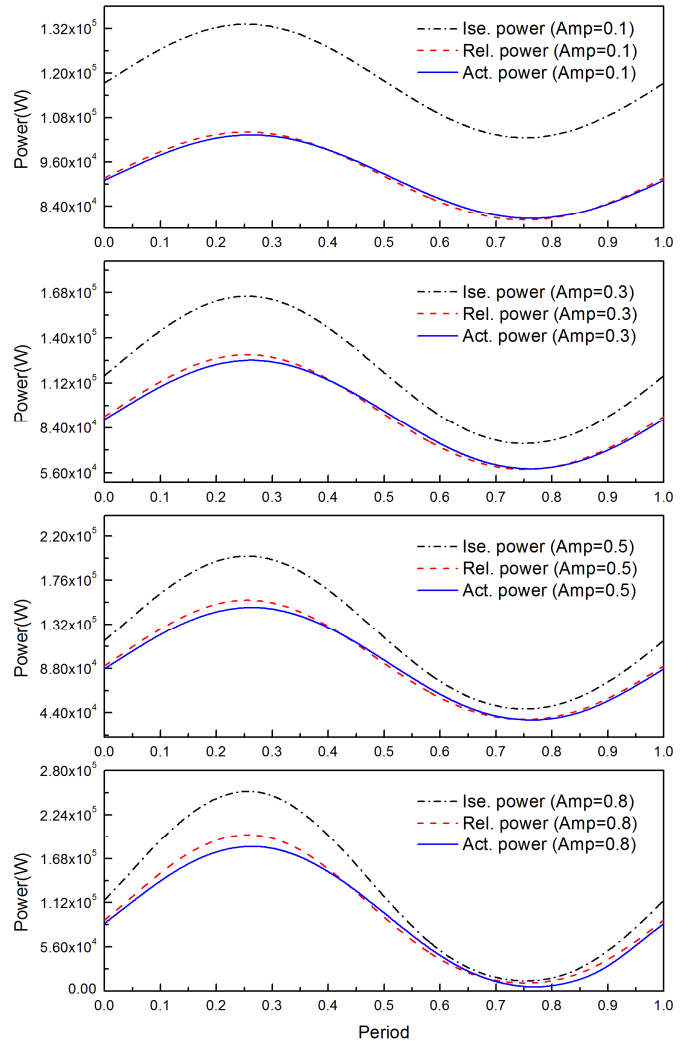


Fig.8 Instantaneous power under different pulsation amplitudes

The simulations were performed under four pulsation amplitudes (Amp=0.1, 0.3, 0.5, 0.8) while keep the pulsation frequency (Fre=75Hz) and average total pressure (Pr=2.0) constant, as shown in Fig.1(b), in order to investigate the effect of the pulsation amplitude on the turbine performance. Fig.8 shows the instantaneous actual power, isentropic power and relative power in one period under different amplitude pulsating flow conditions. Time-average efficiency under the four pulsation amplitudes is listed in Tab.5. Excluding the effect of phase lag, the instantaneous actual power is almost the same as the relative power under the small amplitude pulsation (Amp=0.1), and this lead to the difference between period average efficiency and steady efficiency is only -0.08 percent. When the pulsation amplitude increases, the deviation becomes obvious. In the Amp=0.3 and Amp=0.5 cases, it is also shown that the performance penalty appears in near 1/4 period time region, when the inlet total pressure is high. As the amplitude reaches 0.8, the deviation of actual power from relative power also becomes distinct in low pressure ratio region (near 3/4

period). Corresponding to this, the period average efficiency under 0.8 Amp pulsation is 4.11 percent lower than the steady efficiency under mean pulsation conditions. It is clear that the period average efficiency under all amplitudes is lower than the steady efficiency, and the deviation increases significantly with the pulsation amplitude increasing.

4.3 Effect of pulsation on turbine flow fields

It is shown above that the period average performance of the turbine under pulsating conditions is lower than the steady performance under the mean pulsating conditions, and the instantaneous performance of the turbine fluctuates more seriously when the pulsation amplitude increases. In order to investigate the effect of pulsation on turbine flow fields, the streamlines distribution at 50% span of the turbine under high pulsating conditions ($Pr=2.00$, $Fre=75Hz$, $Amp=0.8$) are plotted in Fig.10. The eight key instants are equally distributed in one period, Fig. 9. It is assumed that the flow fields were periodic from passage to passage, so only two blades are shown in the figures. The blade rotates in the right direction and the leading edge is at the top.

Fig.10 suggests the flow fields fluctuate seriously in one period under the pulsating flow conditions. During the former half period, the instantaneous pressure ratio and mass flow rate are high, so that the blade is exposed to large flow angle and flow separation is observed on the suction surface near the leading edge (t1~t5). The pressure ratio and mass flow rate decreases after t5, and the flow separation on suction surface becomes weak at t6. The inlet total pressure decreases to a minimum value at t7, and the blade is under a large negative flow angle. Hence serious flow separation appears on the pressure side.

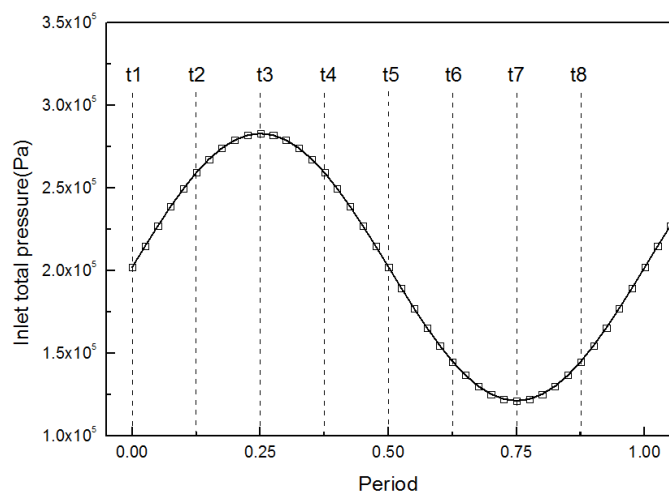


Fig. 9 Eight instants in one period

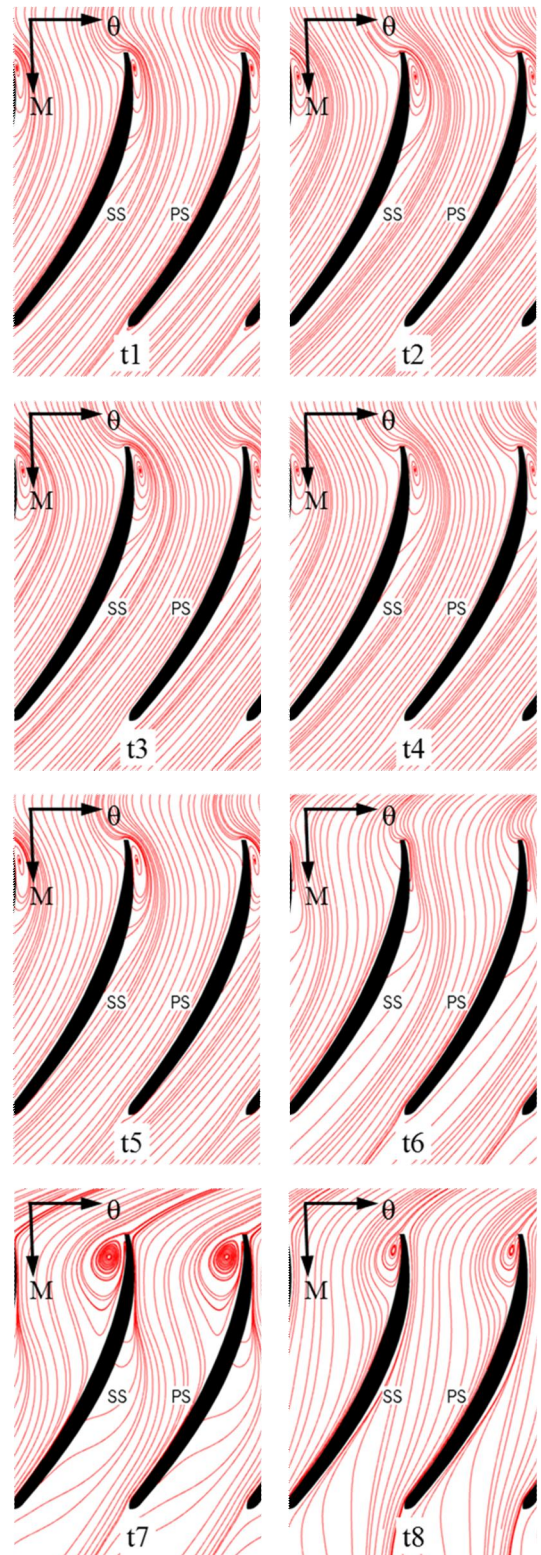


Fig.10 Streamlines at 50% span

According to Fig. 9, the parameters imposed at the inlet boundary are identical at t_6 and t_8 , however there is great difference of flow patterns between these two instants. There is weak flow separation on the suction surface at t_6 , whilst strong reverse flow appears on the pressure surface at t_8 . This demonstrates the unsteady effects of the flow in the turbine under pulsating flow conditions. The different flow patterns of t_6 and t_8 indicate that the flow fields at present are influenced by the flow fields in the past time. The occurrence and vanishing of the vortex are dynamic procedures, and there is hysteresis effect in the unsteady flow. The mass flow and flow angle decrease from t_5 to t_6 , and the flow pattern improves as a result. But influenced by the separation flow at t_5 , there still is weak flow separation on the suction surface at t_6 . Moreover, the separation region is more obvious in the downstream region than the near leading edge region. This is because that the variation of upstream parameters affects the leading edge firstly, then propagates through the blade passage. The reflection of the downstream flow fields is later than the upstream. In like manner, owing to the serious flow pattern at t_7 , the separation flow cannot vanish in an instant and still exists on the pressure side at t_8 , but has an obvious weakening trend. The flow patterns during the former half period are similar, and there mainly is separation flow on the suction surface. Consequently the flow fields hysteresis effect is not so distinct between t_1 and t_5 , as well as between t_2 and t_4 , though the boundary conditions are identical too.

5 CONCLUSIONS

Turbines matched to reciprocating engines are under natural pulsating flow conditions. In order to investigate the effects of the pulsation on the turbine performance, the simulations of the turbine under different kinds of pulsating conditions were performed. The results show that the instantaneous parameters under pulsating flow conditions deviate from the steady condition, and the period average performance of the turbine under pulsating conditions is lower than the steady performance under the mean pulsating conditions.

While the pulsation amplitude and average pressure are kept constant, the phase lag increases as the pulsation frequency increases. Taking the phase lag into consideration, the actual power output varies little with the pulsation frequency changing.

Under the small amplitude pulsation, the instantaneous performance is close to steady performance, and the period average efficiency is almost equal to the steady efficiency. The unsteady characteristics become more obvious when the pulsation amplitude increases. Under the pulsating flow conditions, of which amplitude is 0.8, the period average efficiency is 4.11 percent lower than the steady efficiency. The flow fields fluctuate seriously during the period under this high pulsating flow conditions. The occurrence and vanishing of the vortex are dynamic procedures, and there is hysteresis effect in the unsteady flow.

ACKNOWLEDGMENTS

This work was supported by the National Basic Research Program of China ("973" Program) (Grant No. 2011CB707204) and the National Natural Science Foundation of China (Grant No. 50706020). The authors would like to thank Dr Ricardo Martinez-Botas and his group for their help and providing the experimental data.

REFERENCES

- [1] International Energy Agency, 2010, Key World Energy Statistics 2010.
- [2] Worldwatch Institute, 2004, State of the World 2004: Special Focus: The Consumer Society, WW Norton & Company.
- [3] International Energy Agency, 2010, "CO₂ EMISSIONS FROM FUEL COMBUSTION Highlights (2010 Edition)," No. ISBN-10: 9264061029; ISBN-13: 978-9264061026.
- [4] International Energy Agency, 2009, "World Energy Outlook,".
- [5] Jansen, W., Heitmann, A. M., and Hanawa, M., 2008, "Recovery of automobile engine exhaust energy," ASME Turbo Expo 2008: Power for Land, Sea and Air, American Society of Mechanical Engineers, Berlin, Germany, pp. 733-739.
- [6] Palfreyman, D., and Martinez-Botas, R. F., 2005, "The pulsating flow field in a mixed flow turbocharger turbine: An experimental and computational study," Journal of Turbomachinery, 127(1), pp. 144-155.
- [7] Costall, A., Martinez-Botas, R. F., and Palfreyman, D., 2005, "Detailed study of pulsating flow performance in a mixed flow turbocharger turbine," ASME Turbo Expo 2005: Power for Land, Sea and Air Reno-Tahoe, NV, United States, pp. 1415-1433.
- [8] Hakeem, I., 1995, "Steady and unsteady performance of mixed flow turbines for automotive turbochargers," IMPERIAL COLLEGE LONDON, London, England.
- [9] Karamanis, N., 2000, "Inlet and exit flow characteristics of mixed flow turbines in advanced automotive turbocharging," Imperial College of Science, Technology and Medicine, London, England.
- [10] Chen, L., Zhuge, W., Zhang, Y., Li, Y., and Zhang, S., 2009, "Investigation of flow structure in a turbocharger turbine under pulsating flow conditions," SAE International Journal of Fuels and Lubricants, 1(1), pp. 1167-1174.
- [11] Karamanis, N., 2000, "Inlet and exit flow characteristics of mixed flow turbines in advanced automotive turbocharging," IMPERIAL COLLEGE LONDON.
- [12] SPALART, P. R., and ALLMARAS, S. R., 1992, "A one-equation turbulence model for aerodynamic flows," 30th AIAA Aerospace Sciences Meeting and Exhibit, p. 23.
- [13] Watson, N., and Janota, M. S., 1982, Turbocharging the Internal Combustion Engine, John Wiley & Sons Inc.
- [14] Moustapha, H., Zelesky, M. F., Baines, N. C., and Japiske, D., 2003, Axial and Radial Turbines, Concepts ETI, Inc..
- [15] Mamat, A. M. I. B., and Martinez-Botas, R. F., 2010, "MEAN LINE FLOW MODEL OF STEADY AND PULSATING FLOW OF A MIXED-FLOW TURBINE

TURBOCHARGER," ASME Turbo Expo 2010, American Society of Mechanical Engineers.

[16] Dale, A., and Watson, N., 1986, "VANELESS RADIAL TURBOCHARGER TURBINE PERFORMANCE.," Third International Conference on Turbocharging and Turbochargers., Inst of Mechanical Engineers, London, Engl, London, Engl, pp. 65-76.

[17] Winterbone, D. E., Nikpour, B., and Frost, H., 1991, "A contribution to the understanding of turbocharger turbine performance in pulsating flow," IMechE Paper C433/011.

[18] Baines, N. C., Hajilouy, and B A, Y. J. H., 1994, "The Pulse Flow Performance and Modelling of Radial Inflow Turbines," Fifth International Conference on Turbocharging and Turbochargers.

[19] Szymko, S., 2006, "The development of an eddy current dynamometer for evaluation of steady and pulsating turbocharger turbine performance,", IMPERIAL COLLEGE LONDON, London, England.

[20] Rajoo, S., 2007, "Steady and Pulsating Performance of a Variable Geometry Mixed Flow Turbocharger Turbine,", IMPERIAL COLLEGE LONDON, London, England.

[21] Copeland, C. D., 2009, "The Evaluation of Steady and Pulsating Flow Performance of a Double-entry Turbocharger Turbine,", IMPERIAL COLLEGE LONDON, London, England.